

# A Straight Skeleton Approximating the Medial Axis

Mirela Tănase and Remco C. Veltkamp

Institute of Information & Computing Sciences  
Utrecht University, The Netherlands  
{mirela,Remco.Veltkamp}@cs.uu.nl

**Abstract.** We propose the linear axis, a new skeleton for polygonal shapes. It is related to the medial axis and the straight skeleton, being the result of a wavefront propagation process. The wavefront is linear and propagates by translating edges at constant speed. The initial wavefront is an altered version of the original polygon: zero-length edges are added at reflex vertices. The linear axis is a subset of the straight skeleton of the altered polygon. In this way, the counter-intuitive effects in the straight skeleton caused by sharp reflex vertices are alleviated. We introduce the notion of  $\varepsilon$ -equivalence between two skeletons, and give an algorithm that computes the number of zero-length edges for each reflex vertex which yield a linear axis  $\varepsilon$ -equivalent to the medial axis. This linear axis and thus the straight skeleton can be computed from the medial axis in linear time for polygons with a constant number of “nearly co-circular” sites. All previous algorithms for straight skeleton computation are sub-quadratic.

## 1 Introduction

Skeletons have long been recognized as an important tool in computer graphics, computer vision and medical imaging. The most known and widely used skeleton is the *medial axis* [1]. Variations of it include *smoothed local symmetries* [2] and the *process inferring symmetric axis* [3]. One way to define the medial axis of a polygon  $P$  is as the locus of centers of maximally inscribed disks. Another way to describe it is as the locus of singularities of a propagating wavefront, whose points move at constant, equal speed. The medial axis is also a subset of the Voronoi diagram whose sites are the line segments and the reflex vertices of  $P$ . The medial axis has always been regarded as an attractive shape descriptor. However, the presence of parabolic arcs may constitute a disadvantage for the medial axis. Various linear approximations were therefore proposed. One approach is to use the Voronoi diagram of a sampled set of boundary points [4].

The straight skeleton is defined only for polygonal figures and was introduced by Aichholzer and Aurenhammer [5]. As its name suggests, it is composed only of line segments. Also the straight skeleton has a lower combinatorial complexity than the medial axis. Like the medial axis, the straight skeleton is defined by a wavefront propagation process. In this process, edges of the polygon move inward at a fixed rate.

In [7] a polygon decomposition based on the straight skeleton was presented. The results obtained from the implementation indicated that this technique provides plausible decompositions for a variety of shapes. However, sharp reflex angles have a big impact on the form of the straight skeleton, which in turn has a large effect on the decomposition. Figure 1 shows three examples of the decomposition based on wavefront split events. It clearly shows that the sharp reflex vertices cause a counterintuitive decomposition. The reason why sharp reflex vertices have a big impact on the form of the straight skeleton, is that points in the defining wavefront close to such reflex vertices move much faster than other wavefront points. In contrast, points in the wavefront defining the medial axis move at equal, constant speed (but this leads to the presence of parabolic arcs).

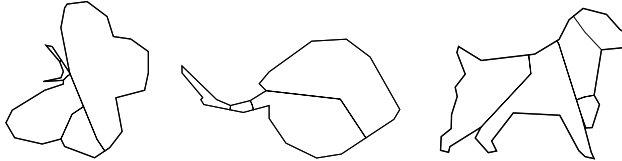


**Fig. 1.** A decomposition [7] based on split events of the straight line skeleton gives counter-intuitive results if the polygon contains sharp reflex vertices.

### 1.1 Contribution

(i) This paper presents the *linear axis*, a new skeleton for polygons. It is based on a linear propagation, like in the straight skeleton. The speed of the wavefront points originating from a reflex vertex is decreased by inserting in the initial wavefront at each reflex vertex a number of zero-length edges, called *hidden edges*. In the propagation, wavefront edges translate at constant speed in a self-parallel manner. The linear axis is the trace of the convex vertices of the propagating wavefront. It is therefore a subset of the straight skeleton of an altered version of the polygon.

(ii) Properties of the linear axis are given in section 3. We compute upper bounds on the speed of the points in the propagating wavefront, that also allows us to identify localization constraints for the skeletal edges, in terms of parabola, hyperbola and Apollonius circles. These properties also prove that the larger the number of hidden edges the better the linear axis approximates the medial axis.

(iii) A thorough analysis of the relation between the number of the inserted hidden edges and the quality of this approximation is given in section 4. We introduce the notion of  $\varepsilon$ -equivalence between the two skeletons. Nodes in the two skeletons are clustered based on a proximity criterion, and the  $\varepsilon$ -equivalence between the two skeletons is defined as an isomorphism between the resulting graphs with clusters as vertices. This allows us to compare skeletons based on their main topological structure, ignoring local detail. We next give an algorithm for computing a number of hidden edges for each reflex vertex such that the resulting linear axis is  $\varepsilon$ -equivalent to the medial axis.

(iv) This linear axis can then be computed from the medial axis. The whole linear axis computation takes linear time for polygons with a constant number

of nodes in any cluster. There is only a limited category of polygons not having this property.

(v) Experimental verification shows that in practice only a few hidden edges are necessary to yield a linear axis that is  $\varepsilon$ -equivalent to the medial axis. Also the resulting decomposition is much more intuitive than the decomposition based on the straight skeleton.

## 2 Skeletons from Propagation

Let  $P$  be a simple, closed polygon. The medial axis  $M(P)$  is closely related to the Voronoi diagram  $VD(P)$  of the polygon  $P$ . The set of sites defining  $VD(P)$  is the set of line segments and reflex vertices of  $P$ . The diagram  $VD(P)$  partitions the interior of  $P$  into Voronoi cells, which are regions with one closest site. The set of points  $U(d)$  inside  $P$ , having some fixed distance  $d$  to the polygon is called a *uniform wavefront*. If  $S$  is an arbitrary site of  $P$ , let  $U_S(d)$  denote the set of points in  $U(d)$  closest to  $S$ . We call  $U_S(d)$  *the (uniform) offset of  $S$* . The uniform wavefront is composed of straight line segments (offsets of line segments) and circular arcs (offsets of reflex vertices) (see figure 2(a)). As the distance  $d$  increases, the wavefront points move at equal, constant velocity along the normal direction. This process is called *uniform wavefront propagation*. During the propagation, the breakpoints between adjacent offsets trace the Voronoi diagram  $VD(P)$ . The medial axis  $M(P)$  is a subset of  $VD(P)$ ; the Voronoi edges incident to the reflex vertices are not part of the medial axis.

The region  $VC(S)$  swept in the propagation by the offset of site  $S$  is the Voronoi cell of  $S$ . It is also the set of points inside  $P$  whose closest site is  $S$ ; the distance  $d(x, S)$  of a point  $x$  to  $S$  is the length of the shortest path inside  $P$  from  $x$  to  $S$ . There are two types of edges in  $M(P)$ : line segments (separating the Voronoi cells of two line segments or two reflex vertices) and parabolic arcs (separating the Voronoi cells of a line segment and a reflex vertex). A *branching node*  $b \in M(P)$  is a node of degree at least three, and the sites whose Voronoi cells intersect in  $b$  are referred to as the *generator sites* of  $b$ . The medial axis contains also nodes of degree two, which will be referred to as the *regular nodes*. They are breakpoints between parabolic arcs and line segments.

The straight skeleton is also defined as the trace of adjacent components of a propagating wavefront. The wavefront is linear and is obtained by translating the edges of the polygon in a self-parallel manner, keeping sharp corners at reflex vertices. In contrast to the medial axis, edges incident to a reflex vertex will grow in length (see figure 2(b)). This also means that points in the wavefront move at different speeds: wavefront points originating from reflex vertices move faster than points originating from the edges incident to those vertices. In fact, the speed of the wavefront points originating from a reflex vertex gets arbitrary large when the internal angle of the vertex gets arbitrary close to  $2\pi$ . Wavefront vertices move on angular bisectors of wavefront edges. The straight skeleton  $SS(P)$  of  $P$  is the trace in the propagation of the vertices of the wavefront.

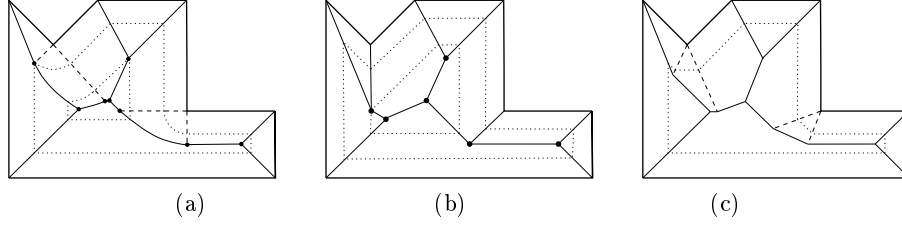


**Fig. 2.** The medial axis (a), the straight skeleton (b) and the linear axis in the case when one hidden edge is inserted at each reflex vertex (c). Instances of the propagating wavefront generating the skeletons are drawn with dotted line style in all cases. In (a) the Voronoi edges that are not part of the medial axis are in dashed line style. In (b) the dashed lines are the bisectors that are not part of the linear axis.

### 3 Linear Axis - definition and properties

In this section we define the *linear axis*. It is based on a linear wavefront propagation like the straight skeleton, but the discrepancy in the speed of the points in the propagating wavefront, though never zero, can decrease as much as wanted. Also, as it turns out from lemma 2, the speed of the points of this wavefront is bounded from above by  $\sqrt{2}$ .

Let  $\{v_1, v_2, \dots, v_n\}$  denote the vertices of a simple polygon  $P$ , and let  $\kappa = (k_1, k_2, \dots, k_n)$  be a sequence of natural numbers. If  $v_i$  is a convex vertex of  $P$ ,  $k_i = 0$ , and if it is a reflex vertex,  $k_i \geq 0$ . Let  $\mathcal{P}^\kappa(0)$  be the polygon obtained from  $P$  by replacing each reflex vertex  $v_i$  with  $k_i + 1$  identical vertices, the endpoints of  $k_i$  zero-length edges, which will be referred to as the *hidden edges* associated with  $v_i$ . The directions of the hidden edges are chosen such that the reflex vertex  $v_i$  of  $P$  is replaced in  $\mathcal{P}^\kappa(0)$  by  $k_i + 1$  “reflex vertices” of equal internal angle. Let  $\mathcal{P}^\kappa(t)$  denote the linear wavefront, corresponding to a sequence  $\kappa$  of hidden edges, at moment  $t$ . The propagation process consists of translating edges at constant unit speed, in a self-parallel manner, i.e. it is the propagation of the wavefront defining the straight skeleton of  $\mathcal{P}^\kappa(0)$ .

**Definition 1.** *The linear axis  $L^\kappa(P)$  of  $P$ , corresponding to a sequence  $\kappa$  of hidden edges, is the trace of the convex vertices of the linear wavefront  $\mathcal{P}^\kappa$  in the above propagation process.*

Obviously,  $L^\kappa(P)$  is a subset of  $SS(\mathcal{P}^\kappa(0))$ ; we only have to remove the bisectors traced by the reflex vertices of the wavefront (see figure 2 (c)). For the rest of this paper, we will assume that each selection  $\kappa$  of hidden edges that is considered, satisfies the condition in the following lemma.

**Lemma 1.** *If any reflex vertex  $v_j$  of internal angle  $\alpha_j \geq 3\pi/2$  has at least one associated hidden edge, then  $L^\kappa(P)$  is an acyclic connected graph.*

A *site* of  $P$  is a line segment or a reflex vertex of the polygon. If  $S$  is an arbitrary site of  $P$ , we denote by  $\mathcal{P}_S^\kappa(t)$  the points in  $\mathcal{P}^\kappa(t)$  originating from  $S$ .

We call  $\mathcal{P}_S^\kappa(t)$  the *(linear) offset of site  $S$  at moment  $t$* . Figure 3(a) illustrates the linear and the uniform offsets of a reflex vertex  $v_j$ , with  $k_j = 3$  associated hidden edges.

Individual points in  $\mathcal{P}^\kappa$  move at different speeds. The fastest moving points in  $\mathcal{P}^\kappa$  are its reflex vertices. The slowest moving points have unit speed (it also means that we assume unit speed for the points in the uniform wavefront). The next lemma gives bounds on the speed of the points in the linear wavefront  $\mathcal{P}^\kappa$ . Let  $v_j$  be a reflex vertex of  $P$ , of internal angle  $\alpha_j$ , and with  $k_j$  associated hidden edges. Let  $\mathcal{P}_{v_j}^\kappa(t)$  be the offset of  $v_j$  at some moment  $t$ .

**Lemma 2.** *Points in  $\mathcal{P}_{v_j}^\kappa(t)$  move at speed at most*

$$s_j = \frac{1}{\cos\left(\frac{\alpha_j - \pi}{2*(k_j + 1)}\right)}.$$

The linear axis  $L^\kappa(P)$  is the trace of the convex vertices of the propagating linear wavefront. Each convex vertex of  $\mathcal{P}^\kappa(t)$  is a breakpoint between two linear offsets. Lemmas 3 and 4 describe the trace of the intersection of two adjacent offsets in the linear wavefront propagation. They are central to the algorithms in section 4. First, we establish the needed terminology. If  $v$  is a vertex and  $e$  is an edge non-incident with  $v$ , we denote by  $P(v, e)$  the parabola with focus  $v$  and directrix the line supporting  $e$ . For any real value  $r > 1$ , we denote by  $H^r(v, e)$  the locus of points whose distances to  $v$  and the line supporting  $e$  are in constant ratio  $r$ . This locus is a hyperbola branch. If  $u$  and  $v$  are reflex vertices, we denote by  $C^r(u, v)$  the Apollonius circle associated with  $u$ , and  $v$ , and ratio  $r \neq 1$ .  $C^r(u, v)$  is the locus of points whose distances to  $u$  and  $v$ , respectively, are in constant ratio  $r$ .

Let  $e$  be an edge and  $v_j$  be a reflex vertex of  $P$  (see figure 3 (b)). The points in the offset  $\mathcal{P}_e^\kappa$  move at unit speed, the points in the offset  $\mathcal{P}_{v_j}^\kappa$  move at speeds varying in the interval  $[1, s_j]$ , where  $s_j$  is given by lemma 2.

**Lemma 3.** *If the linear offsets of  $v_j$  and  $e$  become adjacent, the trace of their intersection is a polygonal chain that satisfies:*

- 1) *it lies in the region between  $P(v_j, e)$  and  $H^{s_j}(v_j, e)$ ;*
- 2) *the lines supporting its segments are tangent to  $P(v_j, e)$ ; the tangent points lie on the traces of the unit speed points in  $\mathcal{P}_{v_j}^\kappa$ ;*
- 3)  *$H^{s_j}(v_j, e)$  passes through those vertices of the chain which lie on the trace of a reflex vertex of  $\mathcal{P}_{v_j}^\kappa$ .*

Let  $v_i$  and  $v_j$  be reflex vertices of  $P$  (see figure 3 (c)). The points in the offset  $\mathcal{P}_{v_i}^\kappa$  move at speeds varying in the interval  $[1, s_i]$ , while the points in the offset  $\mathcal{P}_{v_j}^\kappa$  move at speeds varying in the interval  $[1, s_j]$ .

**Lemma 4.** *If the linear offsets of  $v_i$  and  $v_j$  become adjacent, the trace of their intersection is a polygonal chain that lies outside the Apollonius circles  $C^{s_i}(v_i, v_j)$  and  $C^{s_j}(v_j, v_i)$ .*

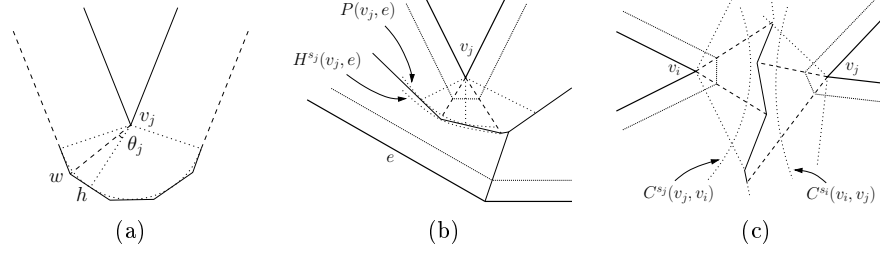


**Fig. 3.** (a) The linear offset (solid line style) of a reflex vertex with 3 associated hidden edges is made of 5 segments tangent to the uniform offset (dotted line style) of this vertex. (b) The linear offsets of reflex vertex  $v_j$  and edge  $e$  trace, in the propagation, a polygonal chain that lies in the region between parabola  $P(v_j, e)$  and hyperbola  $H^{s_j}(v_j, e)$ . (c) The linear offsets of the reflex vertices  $v_i$  and  $v_j$  trace a polygonal chain that lies outside the Apollonius circles  $C^{s_j}(v_j, v_i)$  and  $C^{s_i}(v_i, v_j)$

#### 4 Linear Axis, Topologically Similar to the Medial Axis

Obviously, the larger the number of hidden edges associated with the reflex vertices, the closer the corresponding linear axis approximates the medial axis. For many applications of the medial axis, an approximation that preserves the main visual cues of the shape, though perhaps non-isomorphic to the medial axis, is perfectly adequate. The way we now define the  $\varepsilon$ -equivalence between the medial axis and the linear axis, will allow us to compute a linear axis that closely approximates the medial axis using only a small number of hidden edges.

Let  $\varepsilon \geq 0$ ; an  $\varepsilon$ -edge is a Voronoi edge generated by four almost co-circular sites (see figure 4 (a)). Let  $b_i b_j$  be a Voronoi edge, with  $b_i$  generated by sites  $S_k, S_i, S_l$ , and  $b_j$  generated by  $S_k, S_j, S_l$ .

**Definition 2.** The edge  $b_i b_j$  is an  $\varepsilon$ -edge if  $d(b_i, S_j) < (1 + \varepsilon)d(b_i, S_i)$  or  $d(b_j, S_i) < (1 + \varepsilon)d(b_j, S_j)$ .

A path between two nodes of  $M(P)$  is an  $\varepsilon$ -path if it is made only of  $\varepsilon$ -edges. For any node  $b$  of  $M(P)$ , a node  $b'$  such that the path between  $b$  and  $b'$  is an  $\varepsilon$ -path, is called an  $\varepsilon$ -neighbour of  $b$ . Let  $N_\varepsilon(b)$  be the set of  $\varepsilon$ -neighbours of  $b$ . The set  $\{b\} \cup N_\varepsilon(b)$  is called an  $\varepsilon$ -cluster.

Let  $(V_M, E_M)$  be the graph induced by  $M(P)$  on the set of vertices  $V_M$  composed of the convex vertices of  $P$  and the nodes of degree 3 of  $M(P)$ . Let  $(V_{L^\kappa}, E_{L^\kappa})$  be the graph induced by  $L^\kappa(P)$  on the set of vertices  $V_{L^\kappa}$  composed of the convex vertices of  $P$  and the nodes of degree 3 of  $L^\kappa(P)$ .

**Definition 3.**  $M(P)$  and  $L^\kappa(P)$  are  $\varepsilon$ -equivalent if there exists a surjection  $f : V_M \rightarrow V_{L^\kappa}$  so that:

- i)  $f(p) = p$ , for all convex  $p$  of  $P$ ;
- ii)  $\forall b_i, b_j \in V_M$  with  $b_j \notin N_\varepsilon(b_i)$ ,  $\exists$  an arc in  $E_M$  connecting  $b_i$  and  $b_j \Leftrightarrow \exists$  an arc in  $E_{L^\kappa}$  connecting  $f(b'_i)$  and  $f(b'_j)$  where  $b'_i \in \{b_i\} \cup N_\varepsilon(b_i)$  and  $b'_j \in \{b_j\} \cup N_\varepsilon(b_j)$ .

The following lemma gives a sufficient condition for the  $\varepsilon$ -equivalence of the two skeletons. The *path between two disjoint Voronoi cells*  $VC(S_i)$  and  $VC(S_j)$  is the shortest path in  $M(P)$  between a point of  $VC(S_i) \cap M(P)$  and a point of  $VC(S_j) \cap M(P)$ .

**Lemma 5.** *If the only sites whose linear offsets become adjacent in the propagation, are sites whose uniform offsets trace an edge in the medial axis  $M(P)$  or sites whose path between their Voronoi cells is an  $\varepsilon$ -path, then the linear axis and the medial axis are  $\varepsilon$ -equivalent.*

#### 4.1 Computing a sequence of zero-length edges

We now describe an algorithm for computing a sequence  $\kappa$  of hidden edges such that the resulting linear axis is  $\varepsilon$ -equivalent to the medial axis. As lemma 5 indicates, the linear axis and the medial axis are  $\varepsilon$ -equivalent if only the linear offsets of certain sites become adjacent in the propagation. Namely, those with adjacent Voronoi cells, and those whose path between their Voronoi cells is an  $\varepsilon$ -path. The algorithm handles pairs of sites whose linear offsets must be at any moment disjoint in order to ensure the  $\varepsilon$ -equivalence of the two skeletons. These are sites with disjoint Voronoi cells and whose path between these Voronoi cells is not an  $\varepsilon$ -path. However, we do not have to consider each such pair. The algorithm actually handles the pairs of *conflicting sites*, where two sites  $S_i$  and  $S_j$  (at least one being a reflex vertex) are said to be conflicting if the path between their Voronoi cells contains exactly one non- $\varepsilon$ -edge. When handling a pair  $S_i, S_j$  we check and, if necessary, adjust the maximal speeds  $s_i$  and  $s_j$  of the offsets of  $S_i$  and  $S_j$ , respectively, so that these offsets remain disjoint in the propagation. This is done by looking locally at the configuration of the uniform wavefront and using the localization constraints for the edges of the linear axis given by lemmas 3 and 4. More insight into this process is provided below.

**Handling conflicting sites** Let  $S_i$  and  $S_j$  be a pair of conflicting sites. Let  $b_i \in VC(S_i)$  and  $b_j \in VC(S_j)$  denote the endpoints of the path between their Voronoi cells. The handling of this pair depends on the composition of the path between  $VC(S_i)$  and  $VC(S_j)$ , as well as on the type (reflex vertex or segment) of  $S_i$  and  $S_j$ . A detailed case analysis of all possible combinations is not possible due to space limitations. For this reason, we present here only the structure of the case analysis and detail the handling only in two of these cases. Each of these cases requires a different handling. A complete description can be found in [8].

**A.** The path between the Voronoi cells  $VC(S_i)$  and  $VC(S_j)$  is made of one non- $\varepsilon$ -edge. Let  $S_k$  and  $S_l$  denote the sites whose uniform offsets trace this edge. When handling the pair  $S_i, S_j$  we look locally at the configuration of the uniform wavefront shortly prior to the moment the Voronoi edge  $b_i b_j$  starts being traced in the propagation. We take into consideration not only the type of the sites  $S_i$ , and  $S_j$ , but also the type (regular node or branching node) of  $b_i$  and  $b_j$ .

**A.1.**  $S_i$  is reflex vertex and  $S_j$  is line segment. Regarding  $b_i$  and  $b_j$  we have the following cases:

-  $b_i$  is a branching node and  $b_j$  is a branching or a regular node of  $M(P)$  (see figure 4(b)). The handling of the pair  $S_i, S_j$  in this case is given by:

**Lemma 6.** *If the speed of the points in the linear offset of  $S_i$  is at most  $\frac{d(b_i, S_i)}{d(b_j, S_k)}$ , the linear offsets of  $S_i$  and  $S_j$  are at any moment disjoint.*

-  $b_i$  is a regular node occurring sooner than  $b_j$ , which is a branching node.  
-  $b_i$  is a regular node occurring later than  $b_j$ , which is a regular or branching node.

**A.2.**  $S_i$  and  $S_j$  are reflex vertices. Regarding  $b_i$  and  $b_j$  we distinguish the following cases:

-  $b_i$  and  $b_j$  are branching points. Let  $b$  be the intersection of the perpendicular bisector  $B_{ij}$  of  $S_i$  and  $S_j$  with the edge connecting  $b_i$  and  $b_j$  (see figure 4, (c)). The handling of the pair  $S_i, S_j$  in this case is indicated by:

**Lemma 7.** *If the speed of the points in the linear offset of  $S_i$  is at most  $\frac{d(b, S_i)}{d(b, S_k)}$ , and the speed of the points in the linear offset of  $S_j$  is at most  $\frac{d(b, S_j)}{d(b, S_k)}$ , the linear offsets of  $S_i$  and  $S_j$  are at any moment disjoint.*

-  $b_i$  is a regular node occurring sooner than  $b_j$ , which is a branching node.  
-  $b_i$  is a regular node occurring later than  $b_j$ , which is a branching node.  
-  $b_i$  and  $b_j$  are regular nodes.

**B.** The path between the Voronoi cells  $VC(S_i)$  and  $VC(S_j)$  is made of at least two edges, all except one of them being  $\varepsilon$ -edges. A similar case description as above is omitted due to space limitations.

**Algorithm** The algorithm for computing a sequence  $\kappa$  of hidden edges can now be summarized as follows.

**Algorithm ComputeHiddenEdges ( $P, \varepsilon$ )**

*Input* A simple polygon  $P$  and a constant  $\varepsilon$ .

*Output* The number of hidden edges for each reflex vertex such that the resulting linear axis is  $\varepsilon$ -equivalent to the medial axis.

1. Compute the medial axis  $\mathbf{M}$  of  $P$ .
2. For each reflex vertex  $S_j$  of  $P$ 
  - if**  $\alpha_j \geq 3\pi/2$  **then**  $s_j \leftarrow 1/\cos(\frac{\alpha_j - \pi}{4})$
  - else**  $s_j \leftarrow 1/\cos(\frac{\alpha_j - \pi}{2})$
3. ComputeConflictingSites( $\varepsilon$ )
4. For each pair of conflicting sites  $S_i, S_j$ 
  - $k_j \leftarrow \lceil (\alpha_j - \pi)/(2 \cos^{-1}(1/s_j)) \rceil$ .

In step 1, for each reflex vertex  $S_j$  we initialize the maximal speed  $s_j$  of the reflex vertices in its linear offset. If the angle  $\alpha_j$  of  $S_j$  is greater than  $3\pi/2$ , we associate one hidden edge with  $v_j$ , otherwise the initial number  $k_j$  of hidden edges associated to  $S_j$  is 0 (see section 3). The value of  $s_j$  is then given by lemma 2. In handling a pair of conflicting sites  $S_i, S_j$  in step 3, we use the bounds given by lemmas similar to lemma 6 and 7. After identifying in which of the cases A.1.1-B the conflicting pair falls into, we check whether the current speeds  $s_i$  and/or  $s_j$  satisfy the condition(s) in the corresponding lemma. If they do not, we adjust  $s_i$  and/or  $s_j$  to the bound(s) given by the lemma. Finally in step 4, the



number  $k_j$  of hidden edges associated with each reflex vertex  $S_j$  is determined. It is the smallest number of hidden edges such that the speed of the vertices in the linear offset of  $S_j$  is at most  $s_j$ .

Regarding the computation of the conflicting sites in step 2, we notice that each edge of  $M(P)$ , non-incident to  $P$ , is a path between two Voronoi cells. Thus each non- $\varepsilon$ -edge of  $M(P)$ , non-incident to  $P$ , defines two possibly conflicting sites. What determines whether these are indeed conflicting is the presence of at least one reflex vertex in the pair. If at least one endpoint of the non- $\varepsilon$ -edge is part of an  $\varepsilon$ -cluster, there may be other conflicting sites whose path between their Voronoi cells contains this edge. Their number depends on the number of nodes in the  $\varepsilon$ -clusters of the endpoints of the non- $\varepsilon$ -edge.

**Theorem 1.** *Algorithm ComputeHiddenEdges computes a sequence of hidden edges that leads to a linear axis  $\varepsilon$ -equivalent to the medial axis.*

The performance of the algorithm ComputeHiddenEdges depends on the number of conflicting pairs computed in step 2. This in turn depends on the number of nodes in the  $\varepsilon$ -clusters of  $M(P)$ . If any  $\varepsilon$ -cluster of  $M(P)$  has a constant number of nodes, there are only a linear number of conflicting pairs, since there is a linear number of non- $\varepsilon$ -edges in  $M(P)$ . Each conflicting pair is handled in constant time, thus in this case, ComputeHiddenEdges computes the sequence  $\kappa$  in linear time. There is only a limited class of shapes with a constant number of clusters, each with a linear number of nodes.

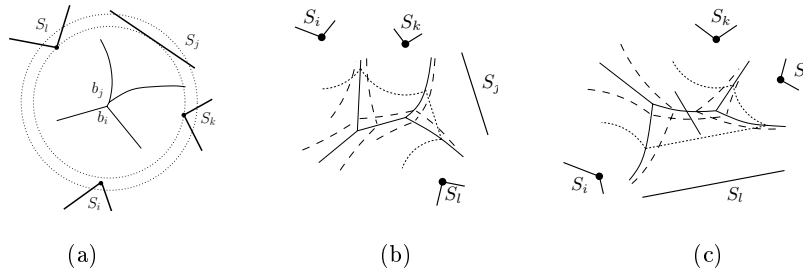


**Fig. 4.** (a) An  $\varepsilon$ -edge  $b_i b_j$  is a Voronoi edge generated by four almost co-circular sites. (b)-(c) Handling the conflicting sites  $S_i$  and  $S_j$  when the path between their Voronoi cells consists of one edge. An instance of the uniform wavefront is drawn in dotted line style, the medial axis in solid line style, and the dashed lines give the localization constraints for the edges in the linear axis.

## 4.2 Computation of the Linear Axis

Once we have a sequence  $\kappa$  that ensures the  $\varepsilon$ -equivalence between the corresponding linear axis and the medial axis, we can construct this linear axis. The medial axis can be computed in linear time [9]. Despite its similarity to the medial axis, the fastest known algorithms for the straight skeleton computation are slower. The first sub-quadratic algorithm was proposed by Eppstein and Erickson [10]. It runs in  $O(n^{1+\epsilon} + n^{8/11+\epsilon} r^{9/11+\epsilon})$  time with a similar space complexity,

where  $r$  is the number of reflex vertices and  $\epsilon$  is an arbitrarily small positive constant. A more recent algorithm by Cheng and Vigneron [11] computes the straight skeleton of a non-degenerate simple polygon in  $O(n \log^2 n + r\sqrt{r} \log r)$  expected time. For a degenerate simple polygon, its expected time bound is  $O(n \log^2 n + r^{17/11+\epsilon})$ . Any of these algorithms can be used to compute the straight skeleton of  $\mathcal{P}^\kappa(0)$ , where  $\mathcal{P}^\kappa(0)$  is the polygon obtained from  $P$  by inserting  $k_j$  zero-length edges at each reflex vertex  $v_j$ . The linear axis  $L^\kappa(P)$  corresponding to the sequence  $\kappa$  is then obtained from  $SS(\mathcal{P}^\kappa(0))$  by removing the bisectors incident to the reflex vertices of  $P$ .

However, if  $M(P)$  has only  $\epsilon$ -clusters of constant size,  $L^\kappa(P)$  can be computed from the medial axis in linear time by adjusting the medial axis. In computing the linear axis, we adjust each non- $\epsilon$ -edge of the medial axis to its counterpart in the linear axis. When adjusting an edge  $b_i b_j$  we first adjust the location of its endpoints to the location of the endpoints of its counterpart. If node  $b_i$  is part of an  $\epsilon$ -cluster, we compute first the counterparts of the nodes in this cluster based on a local reconstruction of the linear wavefront. The adjustment of a node's location is done in constant time, if its  $\epsilon$ -cluster has constant size. Finally, we use lemmas 3 and 4 to replace the parabolic arc or the perpendicular bisector with the corresponding chain of segments. We can now conclude that:

**Theorem 2.** *For a polygon with  $\epsilon$ -clusters of constant size only, a linear axis  $\epsilon$ -equivalent to the medial axis can be computed in linear time.*

## 5 Examples

We have implemented the algorithm `ComputeHiddenEdges` of section 4.1 and the algorithm that constructs the linear axis from the medial axis described in section 4.2. Figure 5 illustrates the straight skeleton (left column), medial axis (middle column) and the linear axis (right column) of the contours of a butterfly, a dog and a ray. The contours come from the MPEG-7 Core Experiment test set “CE-Shape-1”, which contains images of white objects on a black background. The outer closed contour of the object in the image was extracted. In this contour, each pixel corresponds to a vertex. The number of vertices were then decreased by applying the Douglas-Peucker [12] polygon approximation algorithm. For the medial axis computation we used the AVD LEDA package [13], which implements the construction of abstract Voronoi diagrams. The straight skeleton implementation was based on the straightforward algorithm in [14].

For the linear axes in figure 5, the number of hidden edges associated with a reflex vertex is indicated by the number of dashed-line bisectors incident to the reflex vertices that are not part of the linear axis. The difference between the number of incident bisectors and the number of hidden edges is one. We see that a very small number of hidden edges gives a linear axis  $\epsilon$ -equivalent to the medial axis. The counter-intuitive results of the straight skeleton computation for the butterfly and dog are caused by sharp reflex vertices. Only two hidden edges for the reflex vertex between the dog's front legs and for the sharp reflex vertex in the butterfly, are sufficient to get a linear axis  $\epsilon$ -equivalent to the

medial axis. Though the reflex vertices of the ray contour are not very sharp, its straight skeleton indicates why this skeleton is unsuitable as shape descriptor. Two hidden edges associated to each reflex vertex at the body-tail junction, give a linear axis  $\varepsilon$ -equivalent to the medial axis. The largest number of hidden edges in these examples is three, for the reflex vertex between the dog's hind legs.

Figure 6 shows the results of the decomposition of the same contours as in figure 1, but this time based on the split events in the linear axis. We see that the unwanted effects of the sharp reflex vertices are eliminated and the results of this decomposition look more natural.

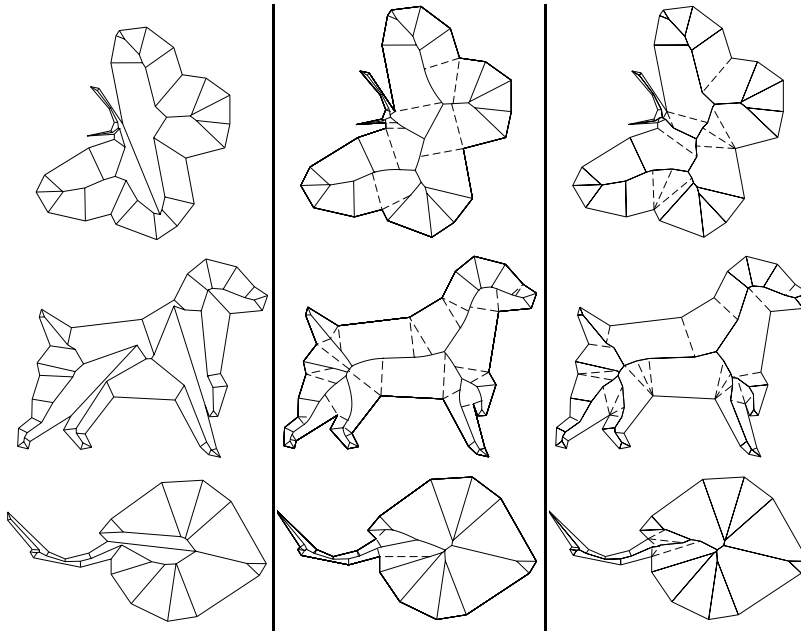


**Fig. 5.** A comparison of the linear axis (right) with the medial axis (middle) and the straight skeleton (left). The dashed lines in the middle column are those Voronoi edges which are not part of the medial axis. The dashed lines in the right column represent the bisectors traced by the reflex vertices of the wavefront, which are not part of the linear axis. In these examples, the linear axis is isomorphic with the medial axis ( $\varepsilon = 0$ ).

## 6 Concluding Remarks

The insertion of zero-length edges at reflex vertices decreases the speed of the wavefront points, which remedies the counter-intuitive effect of sharp reflex vertices in the straight skeleton. Another way to handle sharp reflex vertices could be to allow edges to translate in a non-parallel manner such that the variations in the speed of the wavefronts points are small along the wavefront. It is unclear however how to do this without increasing the complexity of the skeleton, or even if it is possible to do this in such a way that the outcome is a linear

skeleton. Yet another way to take care of sharp reflex vertices is to apply first an outwards propagation, until the sharp reflex vertices have disappeared and then to propagate the front inwards. It is unclear however when to stop the outwards propagation such that relevant reflex vertices are not lost from the wavefront.

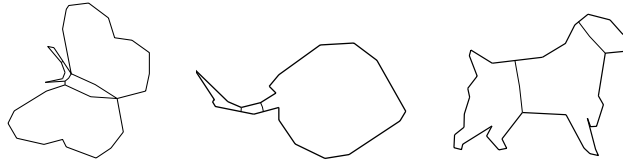


**Fig. 6.** Decompositions based on split events of the linear axis gives natural results even if the polygon contains sharp reflex vertices.

**Acknowledgements:** This research was partially supported by the Dutch Science Foundation (NWO) under grant 612.061.006, and by the FW6 IST Network of Excellence 506766 Aim@Shape.

## References

- [1] Blum, H.: A Transformation for Extracting New Descriptors of Shape. *Symp. Models for Speech and Visual Form*. ed: W. Wathen-Dunn. MIT Press (1967) 362–381.
- [2] Brady, M., Asada, H.: Smoothed Local Symmetries and their Implementation. *The International Journal of Robotics Research* **3(3)** (1984) 36–61.
- [3] Leyton, M.: A Process Grammar for Shape. *Art. Intelligence* **34** (1988) 213–247.
- [4] Ogniewicz, R. L., Kubler, O.: Hierarchic Voronoi Skeletons. *Pattern Recognition* **28(3)** (1995) 343–359.
- [5] Aichholzer, O., Aurenhammer, F.: Straight Skeletons for General Polygonal Figures in the Plane. In: *Proc. 2nd International Computing and Combinatorics Conference COCOON '96*. LNCS Vol. 1090. Springer-Verlag (1996) 117–126.
- [6] Aichholzer, O., Aurenhammer, F., Alberts, D., Gärtner, B.: A Novel Type of Skeleton for Polygons. *The Journal of Universal Computer Science*. **1** (1995) 752–761.
- [7] Tănase, M., Veltkamp, R.C.: Polygon Decomposition based on the Straight Line Skeleton. In: *Proc. 19th ACM Symp. on Computational Geometry*. (2003) 58–67.
- [8] Tănase, M., Veltkamp, R.C.: A Straight Skeleton Approximating the Linear Axis. TR (2004).
- [9] Chin, F., Snoeyink, J., Wang, C.-A.: Finding the Medial Axis of a Simple Polygon in Linear Time. *Discrete Computational Geometry* **21(3)** (1999) 405–420.
- [10] Eppstein, D., Erickson, J.: Raising Roofs, Crashing Cycles, and Playing Pool: Applications of a Data Structure for Finding Pairwise Interactions. *Discrete and Computational Geometry* **22(4)** (1999) 569–592.
- [11] Cheng, S.-W., Vigneron, A: Motorcycle Graphs and Straight Skeletons. In: *Proc. 13th ACM-SIAM Symp. Discrete Algorithms* (2002) 156–165.
- [12] Douglas, D.H., Peucker, T.K.: Algorithms for the Reduction of the Number of Points Required to Represent a Digitized Line or its Caricature. *The Canadian Cartographer* **10(2)** (1973) 112–122.
- [13] AVD LEP, the Abstract Voronoi Diagram LEDA Extension Package. <http://www.mpi-sb.mpg.de/LEDA/friends/avd.html>.
- [14] Felkel, P., Obdržálek, Š.: Straight Skeleton Implementation. In: *Proc. of Spring Conference on Computer Graphics, Budmerice, Slovakia* (1998) 210–218.